JOURNAL OF APPLIED PHYSICS **98**, 123525 (2005)

Characteristics of GaAsN/GaAsSb type-II quantum wells grown by metalorganic vapor phase epitaxy on GaAs substrates

A. A. Khandekar, B. E. Hawkins, and T. F. Kuech
Department of Chemical and Biological Engineering, University of Wisconsin-Madison, 1415 Engineering Drive, Madison, Wisconsin 53706

J. Y. Yeh and L. J. Mawst[a)]
Department of Electrical and Computer Engineering, University of Wisconsin-Madison, 1415 Engineering Drive, Madison, Wisconsin 53706

J. R. Meyer and I. Vurgaftman
Code 5613, Naval Research Laboratory, Washington, D.C. 20375

N. Tansu
Center for Optical Technologies, Department of Electrical and Computer Engineering, Lehigh University, 7 Asa Drive, Bethlehem, Pennsylvania 18015

(Received 2 March 2005; accepted 7 November 2005; published online 29 December 2005)

Pseudomorphic four-period $GaAs_{0.978}N_{0.022}/GaAs_{0.78}Sb_{0.22}$ type-II multiquantum well structures were grown on (100) GaAs substrates by metalorganic vapor phase epitaxy at 530 °C. The $GaAs_{0.978}N_{0.022}$ layers were grown at a V/III ratio of 685 and N/V ratio of 0.96, whereas the $GaAs_{0.78}Sb_{0.22}$ was grown at a V/III ratio of 3.8 and Sb/V ratio of 0.8. The superlattice peaks in the x-ray diffraction θ-2θ scans around the (400) GaAs peak were fitted using a dynamical simulation model to determine layer thickness and alloy compositions. The GaAsN and GaAsSb thicknesses were ~8 nm and ~5 nm, respectively. The photoluminescence (PL) spectra were obtained at 30 K and the PL peak energy was found to match the type-II transition energy obtained from a 10-band $\mathbf{k}\cdot\mathbf{p}$ model. Postgrowth annealing under arsine-H_2 with a N_2 cooldown was found to increase the low temperature PL intensity and result in the appearance of luminescence at room temperature.
© *2005 American Institute of Physics*. [DOI: 10.1063/1.2148620]

I. INTRODUCTION

The active regions of conventional diode lasers that achieve 1.55-μm wavelength operation are based on InGaAs- or InGaAsP-multiple quantum wells (MQWs) on InP-substrates.[1,2] Unfortunately, these lasers show high temperature sensitivity,[1,2] due to several factors, which include Auger recombination, carrier leakage, intravalence band absorption (IVBA), and a strong temperature dependence of the material gain. The temperature sensitivity of the active region *and* the difficulty of forming high-quality distributed Bragg reflectors (DBRs) for the realization of vertical cavity surface emitting lasers (VCSELs) on InP substrates have led to the exploration of 1.55-μm-emitting active regions that can be grown on GaAs substrates.

The active material InGaAsN is one of the strongest candidates for GaAs-based lasers emitting above 1.3 μm.[3] Studies of wavelength extension using InGaAsN active regions have successfully realized lasers with wavelengths beyond 1.4 μm.[4,5] Furthermore, the addition of antimony into InGaAsN during molecular beam epitaxy (MBE) growth[6,7] has been utilized to achieve GaInNAsSb quantum-well (QW) lasers emitting at 1.49 μm, with a low threshold current density of 1.1 kA/cm^2.[7] However, these works have all employed MBE growth techniques.[4–7]

The pursuit of InGaAsN QW lasers grown by MOCVD has led to high-performance diodes with record low-threshold current densities of 200–210 A/cm^2 for emission wavelengths in the 1280–1320 nm range.[8] InGaAsN lasers grown by metalorganic vapor phase epitaxy (MOVPE) have been limited to $\lambda = 1.38$ μm, where the threshold current density was 2.2 kA/cm^2.[9] However, MOVPE structures with InGaAsN QWs and GaAsN barriers have recently demonstrated record low threshold current densities for $\lambda = 1.378$, and InGaAsN lasers with carefully chosen QW growth condition, barrier material and annealing temperature have achieved lasing to $\lambda = 1.41$ μm. Threshold current densities were 563 and 1930 A/cm^2 for the lasers emitting at $\lambda = 1.378$ and 1.41 μm, respectively.[10–12]

Type-II quantum wells, which have been implemented in mid-IR diode lasers on GaSb substrates,[13] offer another potential solution to the problem of achieving long-wavelength emission on GaAs. The energy gap in a type-II structure is governed primarily by the relative conduction and valence band alignments in the two adjacent layers, rather than by the bulk gap in a single layer. In principle, the resulting flexibility comes at the expense of reduced overlap between the electron and hole wave functions that now peak in different layers. On GaAs substrates, InGaAs/GaAsSb type-II QWs have been proposed and implemented for $\lambda = 1.3$ μm lasers.[14] However, further wavelength extension is difficult, due to the high compressive strain of the InGaAs and GaAsSb layers.

We recently discussed[15,16] an alternate approach for

[a)]Electronic mail: mawst@engr.wisc.edu

 © 2005 American Institute of Physics

Downloaded 20 Jul 2011 to 128.180.137.141. Redistribution subject to AIP license or copyright; see http://jap.aip.org/about/rights_and_permissions

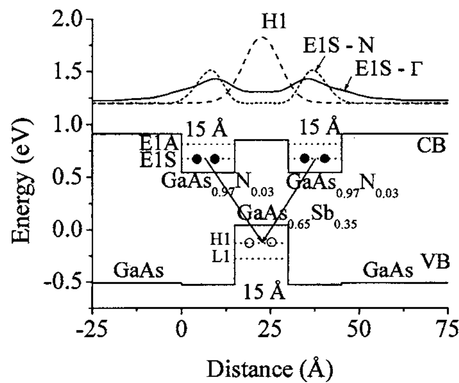

FIG. 1. Schematic energy band diagram for the active region of the proposed dilutenitride type-II "W" laser.

achieving 1.55 μm emission on a GaAs substrate, based on an (In)GaAsN/GaAsSb–GaAs dilute-nitride version of the type-II "W" configuration.[13] These dilute nitride type-II W structures offer the combination of built-in strain compensation, strong carrier confinement, and large electron-hole overlap. This approach has the potential for realizing high-performance monolithic GaAs-based VCSELs, as well as reduced temperature sensitivity edge-emitting lasers for the 1.55 μm wavelength region.

The schematic energy band diagram of a GaAsN/GaAsSb/GaAs type-II W active region optimized for emission at $\lambda = 1.55$ μm is shown in Fig. 1. The conduction band minimum is in the $GaAs_{0.97}N_{0.03}$ electron QWs, while the valence band maximum is in the $GaAs_{0.65}Sb_{0.35}$ hole QWs. Such a design is possible due to the large disparity between the GaAsN and GaAsSb band lineups and that of GaAs.[17] As shown by Wu *et al.*,[18] GaAsN has a very small negative valence band offset (ΔE_v) of 20 meV/%N. The weakly type-II lineup of the GaAsN/GaAs valence bands results in a large conduction band offset, e.g., $\Delta E_c \approx 350$ meV for $N=0.03$. It has been reported that GaAsSb/GaAs has a transition to type-II lineup of the conduction bands at Sb=0.43, with relatively weak type-I alignment for Sb=0.35 resulting in a large ΔE_v of $\sim$500 meV.[19,20]

In contrast to previous InGaAs/GaAsSb type-II designs[14] for $\lambda = 1.3-1.55$ μm, our structure has the potential advantage of offering strain compensation, since it combines tensile-strained GaAsN with compressively strained GaAsSb. This would allow any number of the multiple QWs to be incorporated into the design without sacrificing material quality. Another advantage is the strong confinement of both electrons and holes in their respective wells. The electrons in the GaAsN QWs are sandwiched by GaAs and GaAsSb layers with large ΔE_c, while the holes in the GaAsSb are confined by the large ΔE_v of the GaAsN. Our simulations[15] project that lasers with the GaAsN/GaAsSb type-II W QWs can potentially realize high-temperature and high-power operation due to the strong carrier confinement coupled with the potential for minimal Auger nonradiative decay.[13]

In this paper, we present preliminary results from MOVPE growth and optical characterization of GaAsN/GaAsSb type-II QW structures. The observation of room-temperature photoluminescence (PL) at wavelengths near 1.43 μm demonstrates the type-II nature of the transitions. We find good agreement of the PL peak wavelength with calculations based on a 10-band $\mathbf{k}\cdot\mathbf{p}$ formalism. A strong effect of the thermal annealing conditions on the room temperature PL intensity is also established.

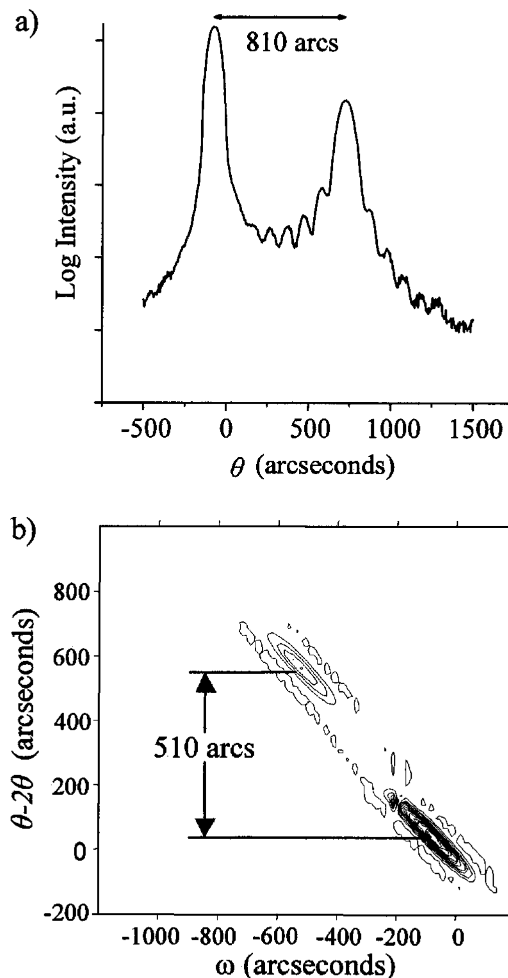

FIG. 2. (a) XRD (400) θ-2θ scan and (b) (311) reciprocal space map for a 0.25-μm-thick GaAsN film.

II. EXPERIMENTAL METHODS

GaAsSb and GaAsN layers were grown in a horizontal MOVPE reactor operated at 78 Torr. Trimethyl gallium (TMGa), trimethyl antimony (TMSb), 1,1-dimethyl hydrazine (DMHz), and arsine were used as the Ga, Sb, N, and As precursors, respectively, in Pd-diffused H_2 carrier gas. Semi-insulating (SI) epiready GaAs (100) wafers without an intentional miscut were used as the substrates. Prior to the growth, the substrates were annealed in arsine at 650 °C for 10 min to desorb any surface oxides. The temperature was subsequently ramped down to the growth temperature of 530 °C under an arsine environment. A 30-nm-thick initial layer of GaAs was grown before the alloy-layer growth. Thick layers of GaAsN were grown at a V/III ratio of 740, with a N/V ratio of 0.89. The thick-layer samples were characterized using on-axis (400) x-ray diffraction (XRD) θ-2θ scans and

Downloaded 20 Jul 2011 to 128.180.137.141. Redistribution subject to AIP license or copyright; see http://jap.aip.org/about/rights_and_permissions

off-axis (311) reciprocal space mapping to determine the strain state and the composition of the GaAsN layers. Electron microprobe analysis (EMPA) was also carried out, to determine N concentration in the thick layers. The As/III ratio was then decreased in a stepwise manner to achieve desired N concentrations in the GaAsN films. Four-period pseudomorphic GaAs/GaAsN superlattice (SL) were grown under varying As/III ratios. The growth time for a GaAs layer was 34 s, while that for a GaAsN layer was 8 s. θ-2θ XRD scans were obtained around the (400) substrate peak and the SL peaks were fitted to a dynamical simulation model to determine the layer thickness and N concentration. This information was then used to calibrate the growth rate and composition of GaAsN layers. A V/III ratio of 684 and N/V ratio of 0.96 resulting in 2.3% N incorporation in the films was chosen for growth of GaAsN/GaAsSb type II SLs.

The pseudomorphic GaAsSb layers in the type-II MQW structure were grown at a V/III ratio of 3.8 and Sb/V ratio of 0.8, which resulted in 20% Sb incorporation. The gas switching sequence was optimized to produce the most abrupt interfaces between the alloy layers. That sequence consisted of 5 s of TMSb and H_2 exposure prior to the GaAsSb growth and 1 s of TMGa in H_2 followed by 5 s of arsine and DMHz exposure prior to the GaAsN growth. The optimal gas-switching sequence for reproducibly inducing minimal Sb compositional grading in the GaAsSb layers of pseudomorphic GaAs–$GaAs_{0.8}Sb_{0.2}$ SLs was established in a separate study.[21]

Four periods of a $GaAs_{0.78}Sb_{0.22}/GaAs_{0.978}N_{0.022}$ type II SL were grown using the above-mentioned optimized conditions. XRD θ-2θ scans and dynamical simulations were used to determine the layer thicknesses and compositions, and transmission electron microscopy (TEM) was performed in cross section to confirm the layer thicknesses. The samples were subjected to various postgrowth annealing treatments, which consisted of annealing under arsine-H_2 and N_2. The cooldown ambient after the arsine anneals was varied between arsine-H_2 and N_2. Photoluminescence spectroscopy was performed on the as-grown and annealed samples, using a cooled Ge detector and lock-in amplifier. The 10-band $\mathbf{k}\cdot\mathbf{p}$ model was used to calculate QW transition energies in the type II structure.

III. RESULTS

Figures 2(a) and 2(b) present the (400) XRD θ-2θ scan and (311) reciprocal space map (RSM), respectively, for a 0.25-μm-thick GaAsN film grown at a V/III ratio of 740 and N/V ratio of 0.89. The peak splitting along the 2θ axis in the RSM was used to calculate d_{311} for the GaAsN lattice. This d_{311} and the out-of-plane lattice constant, d_{100}, obtained from the (400) θ-2θ scans were then used to determine the in-plane lattice constant of the GaAsN film. The film in-plane lattice constant was found to match the lattice constant of bulk GaAs. This coherency of the lattice at the interface indicated that the GaAsN film was completely strained at its 250 nm thickness. Using Vegard's law and assuming a Poisson's ratio of 0.25 for the strained film, the N concentration

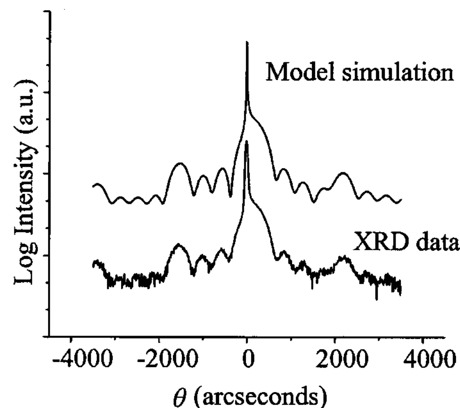

FIG. 3. XRD high-resolution θ-2θ scan around the (400) Bragg peak (bottom) and a dynamical simulation (top) for a 8.4 nm GaAs/1.9 nm $GaAs_{0.973}N_{0.027}$ four period SL.

was found to be 0.016. The electron microprobe analysis yielded a consistent N composition of 1.6±0.6%.

A pseudomorphic four-period GaAs/GaAsN SL structure was grown at the same growth conditions. XRD θ-2θ scans were obtained, and the SL peaks were fitted to a dynamical simulation model to determine the individual layer thicknesses. Samples grown with decreasing arsine flow to the reactor were found to have increasing N concentration in the GaAsN films. Figure 3 shows the experimental θ-2θ scan for a GaAs/GaAsN SL structure grown at a V/III ratio of 665 and N/V ratio of 0.99, along with the fitted dynamical simulation. The presence of second and higher order diffraction peaks indicated that the interfaces between the layers were uniform and smooth. The GaAsN layer thickness and N concentration were determined from the fit to be 1.9 nm and 0.027, respectively.

The $GaAs_{0.978}N_{0.022}$ layers of a four-period type-II GaAsN/GaAsSb SL were grown at a V/III ratio of 685 and N/V ratio of 0.96. Figure 4 shows the experimental XRD θ-2θ scan and dynamical simulation for a four period $GaAs_{0.978}N_{0.022}/GaAs_{0.78}Sb_{0.22}$ SL sample. The growth time for the GaAsN layer was 18 s, whereas the GaAsSb layer was grown for 53 s. The fit to the x-ray data indicated $GaAs_{0.78}Sb_{0.22}$ and $GaAs_{0.978}N_{0.022}$ layer thicknesses of 4.9 and 7.2 nm, respectively. A cross-sectional bright field strain-

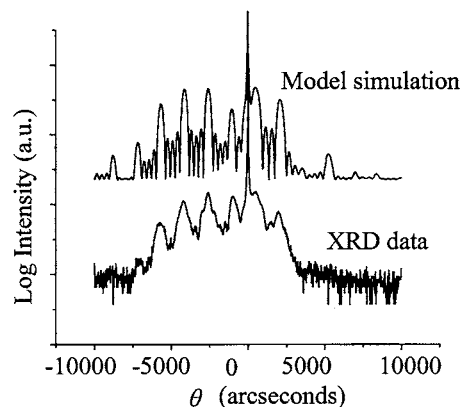

FIG. 4. XRD high-resolution θ-2θ scan around the (400) Bragg peak (bottom) and a dynamical simulation (top) for a 4.9 nm $GaAs_{0.78}Sb_{0.22}$/7.2 nm $GaAs_{0.978}N_{0.022}$ four period SL.

Downloaded 20 Jul 2011 to 128.180.137.141. Redistribution subject to AIP license or copyright; see http://jap.aip.org/about/rights_and_permissions

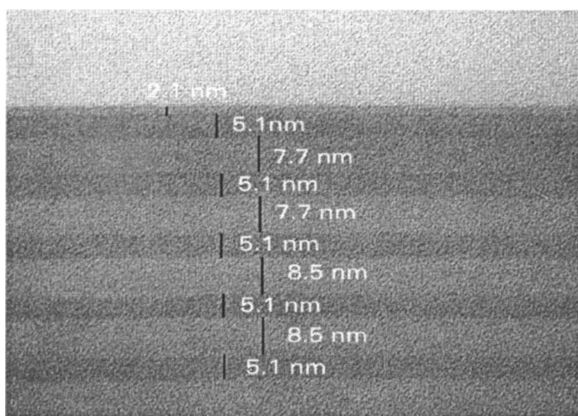

FIG. 5. Cross-sectional BF TEM micrograph of a 4.9 nm $GaAs_{0.78}Sb_{0.22}$/7.8 nm $GaAs_{0.978}N_{0.022}$ four period SL.

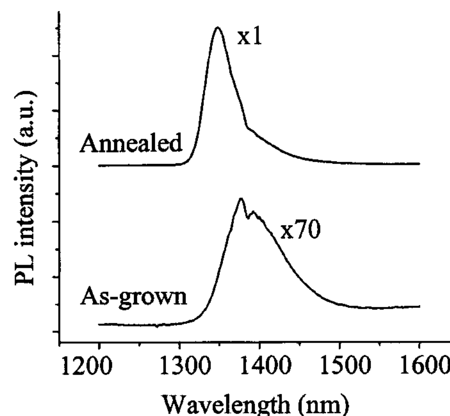

FIG. 7. 30 K PL spectra from as-grown (bottom) and annealed (top) 5.7 nm $GaAs_{0.978}N_{0.022}$/4.3 nm $GaAs_{0.78}Sb_{0.22}$ four period SL.

contrast image of the same GaAsN-GaAsSb sample is depicted in Fig. 5. The average GaAsN and GaAsSb layer thicknesses determined from six TEM images were found to closely match the XRD values. Considerable nonuniformity of the layer thickness was observed across each wafer and among different growth runs. The GaAsSb thickness ranged between 4.3 and 5.9 nm, whereas the GaAsN thickness varied from 5.9 to 8.3 nm across different runs.

PL spectra obtained at 30 K from as-grown and annealed SL samples with 8 nm GaAs/2 nm $GaAs_{0.984}N_{0.016}$ are shown in Fig. 6. The PL peak intensity increases twofold after the annealing treatment, indicating that the alloy layer experiences small changes in the optical and electrical properties upon annealing. The transition energy for the type-I SL calculated assuming a perfect valence band lineup between GaAs and $GaAs_{0.984}N_{0.016}$ was 1.44 eV, which matches well with the experimental peak energy of 1.39 eV. PL spectra obtained from the 5.7 nm $GaAs_{0.978}N_{0.022}$/4.3 nm $GaAs_{0.78}Sb_{0.22}$ type II SL sample are shown in Fig. 7. The upper curve was obtained after the sample was annealed for 30 min at 640 °C in arsine-H_2 and cooled down under N_2 ambient. Comparison with the PL from the same as-grown sample before annealing (lower curve) shows that the annealing produced a 70-fold increase in the intensity. On the other hand, RTA at 500 °C for 1 min resulted in a threefold decrease in the PL intensity. No room temperature (RT) PL signal was observed from any of the as-grown type-II SLs. Following annealing under arsine-H_2 with a N_2 cooldown, however, the type-II sample yielded the RT PL spectrum shown in Fig. 8. The peak wavelength was found to be about 1425 nm. The origin of the small peak at ~1200 nm is unknown, and does not match with simulated energy for the transition between GaAsN and GaAs clad layer.

Theoretical energy gaps were derived from the 10-band $\mathbf{k}\cdot\mathbf{p}$ formalism. The calculated results for the type-II GaAsN/GaAsSb SL structures were in good agreement with the experimental PL data, especially before the annealing treatment. Sb and N compositions obtained from the XRD simulation fits were used for calculation of transition energies. For example, the theoretical energy gaps for the structure of Figs. 7 and 8 are 1419 and 1515 nm at the temperatures of 30 and 300 K, respectively. Good agreement was also obtained for a series of type-I GaAs/GaAsSb SLs emitting at wavelengths in the 1.0–1.2 μm range.[21] Furthermore, the calculated energy gap of 1043 nm for a 6 nm $GaAs_{0.975}N_{0.025}$ QW surrounded by thick GaAs barriers reproduced closely the experimental PL peak. The simulated peak positions, taken together with the PL data in Figs. 6–8, confirm that the transition observed in the $GaAs_{0.78}Sb_{0.22}$/$GaAs_{0.978}N_{0.022}$ SL indeed has a type-II nature, i.e., with staggered conduction and valence band edges. We emphasize that the dilute nitride type-II structures dis-

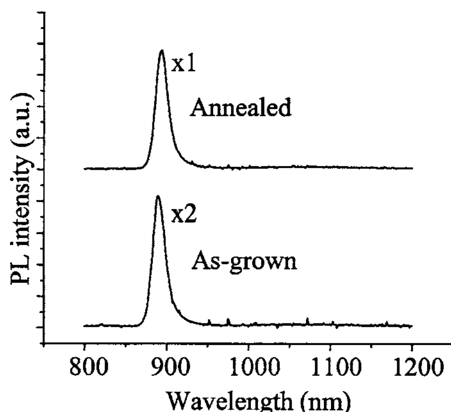

FIG. 6. 30 K PL spectra from as-grown (bottom) and annealed (top) 8 nm GaAs/2 nm $GaAs_{0.084}N_{0.016}$ four period SL.

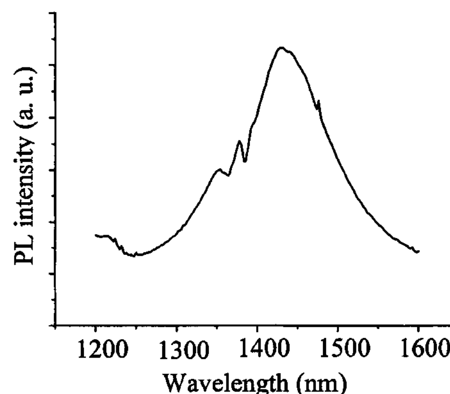

FIG. 8. Room temperature (300 K) PL spectrum from the annealed four period GaAsSb/GaAsN SL sample of Fig. 7.

Downloaded 20 Jul 2011 to 128.180.137.141. Redistribution subject to AIP license or copyright; see http://jap.aip.org/about/rights_and_permissions

cussed in this article produce photoemission at much longer wavelengths than either the GaAs/GaAsSb or InGaAs/GaAs SLs.

IV. CONCLUSIONS

PL peak energies in the vicinity of the 1.55 μm wavelength region were obtained from GaAsN/GaAsSb type-II SL structures grown by MOVPE. Post-growth annealing is found to substantially improve the optical properties of the alloy layers. Annealing increases the PL intensity at 30 K by a factor of 70, and yields a substantial signal at room temperature. Optimization of the type-II structure, in terms of higher Sb content and thinner QWs will induce both longer-wavelength emission and enhanced electron-hole wave function overlap.

ACKNOWLEDGMENTS

The authors would like to thank the Army Research Office (ARO) for their funding support.

[1]Y. Zou, J. S. Osinski, P. Grodzinski, P. D. Dapkus, W. C. Rideout, W. F. Sharfin, J. Schlafer, and F. D. Crawford, IEEE J. Quantum Electron. **29**, 1565 (1993).
[2]A. F. Phillips, A. F. Sweeney, A. R. Adams, and P. J. A. Thijs, IEEE J. Sel. Top. Quantum Electron. **5**, 401 (1999).
[3]M. Kondow, T. Kitatani, S. Nakatsuka, M. C. Larson, K. Nakahara, Y. Yazawa, M. Okai, and K. Uomi, IEEE J. Sel. Top. Quantum Electron. **3**, 719 (1997).
[4]D. Gollub, M. Fischer, and A. Forchel, Electron. Lett. **38**, 1183 (2002).
[5]J. A. Wei, F. N. Xia, C. Q. Li, and S. R. Forrest, IEEE Photonics Technol. Lett. **14**, 597 (2002).
[6]H. Shimizu, K. Kumada, S. Uchiyama, and A. Kasukawa, IEEE J. Sel. Top. Quantum Electron. **7**, 355 (2001).
[7]S. R. Bank, M. A. Wistey, H. B. Yuen, L. L. Goddard, W. Ha, and J. S. Harris, Electron. Lett. **39**, 1445 (2003).
[8]N. Tansu, N. J. Kirsch, and L. J. Mawst, Appl. Phys. Lett. **81**, 2523 (2002).
[9]F. Hohnsdorf, J. Koch, S. Leu, W. Stolz, B. Borchert, and M. Druminski, Electron. Lett. **35**, 571 (1999).
[10]J. Yeh, L. J. Mawst, and N. Tansu, J. Cryst. Growth **272**, 719 (2004).
[11]N. Tansu, J. Y. Yeh, and L. J. Mawst, J. Phys.: Condens. Matter **16**, S3277 (2004).
[12]J. Y. Yeh, N. Tansu, and L. J. Mawst, Electron. Lett. **40**, 739 (2004).
[13]J. R. Meyer, C. A. Hoffman, F. J. Bartoli, and L. R. Ram-Mohan, Appl. Phys. Lett. **67**, 757 (1995); M. Kim, W. W. Bewley, J. R. Lindle, C. S. Kim, I. Vurgaftman, J. R. Meyer, J. G. K. Kim, and R. U. Martinelli, Appl. Phys. Lett. **83**, 5374 (2003).
[14]P. Dowd, W. Braun, D. J. Smith, C. M. Ryu, C.-Z. Guo, S. L. Chen, U. Koelle, S. R. Johnson, and Y.-H. Zhang, Appl. Phys. Lett. **75**, 1267 (1999).
[15]N. Tansu and L. J. Mawst, IEEE J. Quantum Electron. **39**, 1205 (2003).
[16]I. Vurgaftman, J. R. Meyer, N. Tansu, and L. J. Mawst, Appl. Phys. Lett. **83**, 2742 (2003).
[17]I. Vurgaftman and J. R. Meyer, J. Appl. Phys. **94**, 3675 (2003).
[18]J. Wu, W. Shan, W. Walukiewicz, K. M. Yu, J. W. Ager III, E. E. Haller, H. P. Xin, and C. W. Tu, Phys. Rev. B **64**, 085320 (2001).
[19]G. Liu and S.-L. Chuang, J. Appl. Phys. **88**, 5554 (2000).
[20]J.-B. Wang, S. R. Johnson, S. A. Chaparro,† D. Ding, Y. Cao, Yu. G. Sadofyev, and Y.-H. Zhang, Phys. Rev. B **70**, 195339 (2004).
[21]B. E. Hawkins, A. A. Khandekar, J. Y. Yeh, L. Mawst, and T. F. Kuech, J. Cryst. Growth **272**, 686 (2004).

Downloaded 20 Jul 2011 to 128.180.137.141. Redistribution subject to AIP license or copyright; see http://jap.aip.org/about/rights_and_permissions